POLITECNICO DI TORINO
Repository ISTITUZIONALE

Lead-Lag Filter-Based Damping of Virtual Synchronous Machines

(Article begins on next page)

07 August 2024

Lead-Lag Filter-based Damping of Virtual Synchronous Machines

Fabio Mandrile, *Member, IEEE*, Vincenzo Mallemaci, *Student Member, IEEE*,
Enrico Carpaneto, *Member, IEEE*, and Radu Bojoi, *Fellow, IEEE*

Abstract—Traditional power systems based on synchronous generators often feature low frequency electromechanical oscillations. However, the integration of renewable energy sources through power converters can help tackling this issue. In fact, thanks to the concept of virtual synchronous machine (VSM), it is possible to make the inverters behave as real synchronous machines (SMs). This way, the inverters can be integrated into the grid as traditional SMs and can even outperform them when it comes to damping low frequency oscillations in the power system. To do that, proper damping algorithms must be adopted in the VSM model. Therefore, this paper presents a simple and straightforward damping method for VSMs based on a single lead-lag filter acting on the VSM active power feedback. The proposed method and its integration in the VSM model are described. Moreover, a comparison method and four performance indices are proposed, to better evaluate the performance of the VSM damping methods. Finally, the proposed solution has been experimentally compared to five conventional methods to highlight its features according to the proposed performance indices.

Index Terms—Electromechanical Damping, Lead-lag filter, Renewable Energy Sources, Virtual Synchronous Machine (VSM)

I. INTRODUCTION

Modern power systems are facing the challenge of integrating renewable energy sources (RESs) into the electric grid. Differently from traditional synchronous sources (e.g., thermal plants), many RESs are interfaced to the grid through power converters. Most control methods available for these sources are based on maximum power point tracking (MPPT) algorithms, with the goal of always injecting the maximum power available on the source side. However, this MPPT logic relies on the still prevalent presence of synchronous machines (SMs) in the grid and it may lead to frequency stability issues under large penetration of RESs. To tackle this issue, it is possible to make static converters more grid friendly, using proper control algorithms, such as the concept of virtual synchronous machine (VSM) [1], [2]. This way, electronic converters are enabled to provide key ancillary services to the grid, such as virtual inertia and reactive support during grid faults. Moreover, VSMs have some key advantages compared to real SMs. First, VSMs do not have the physical electromagnetic limitations of real SMs (e.g., saturation, couplings, etc...) and their parameters can be adapted to the instantaneous grid conditions, being digital control algorithms. Second, the

F. Mandrile, V. Mallemaci, E. Carpaneto and R. Bojoi are with the Dipartimento Energia "G. Ferraris", Politecnico di Torino, Torino, 10129, Italy (e-mail: fabio.mandrile@polito.it)

dynamic behavior of VSMs is much faster than SMs, as it only depends on the digital control bandwidth (hundreds of Hz or kHz) and it is not limited by the thermal and mechanical transients of traditional plants (e.g., thermal power plants).

Therefore, while SMs are affected by a limited electromechanical damping and cannot easily counteract low frequency power oscillations (range few Hz) due to the limited dynamics of their prime movers (e.g., thermal plants), VSMs are capable of tackling these issues and improving the performance of the power system in terms of oscillations damping.

However, in order to accomplish this goal, it is necessary to implement an effective damping algorithm in the VSM model. To this purpose, several strategies have been reported in the technical literature [3]:

- Damping implemented in the emulated swing equation [4] of the VSM, proportional to the difference between the VSM speed and the nominal grid frequency [5] (droop-damping);
- Damping proportional to the speed difference between the VSM and the actual grid frequency measured by a phase locked loop (PLL) [6] (PLL-damping);
- Damping power proportional to the VSM virtual acceleration [7];
- Virtual dampers and modified virtual impendances [8]–[10];
- Droop-damping method enhanced with a high-pass filter (HP-damping) [11], [12].

While all these methods guarantee the necessary damping to VSMs, they often suffer of several drawbacks, such as the coupling between the damping and the active droop action [10], an altered inertial behavior of the VSM [11], [12], the need of an additional phase locked loop (PLL) [6], numerical derivatives [3] or additional non necessary complexity added to the model, such as the modification of the virtual stator circuit [9]. An appealing solution to provide damping is based on lead-lag filters, which are well known in the field of power systems modeling and grid converter control. So far, these filters are currently mainly used either to describe the physical behavior of parts of power generation units (e.g., the governor of synchronous generators) [4] or to improve the response of conventional grid-connected converters implementing droop control [13], [14]. A notable application of lead-lag filters to VSMs is [15], where the inertial part of the VSM is replaced by a lead-lag filter. This solution enables good damping performance while integrating a tunable frequency droop control. However, the lead-lag filters are mainly used to improve the
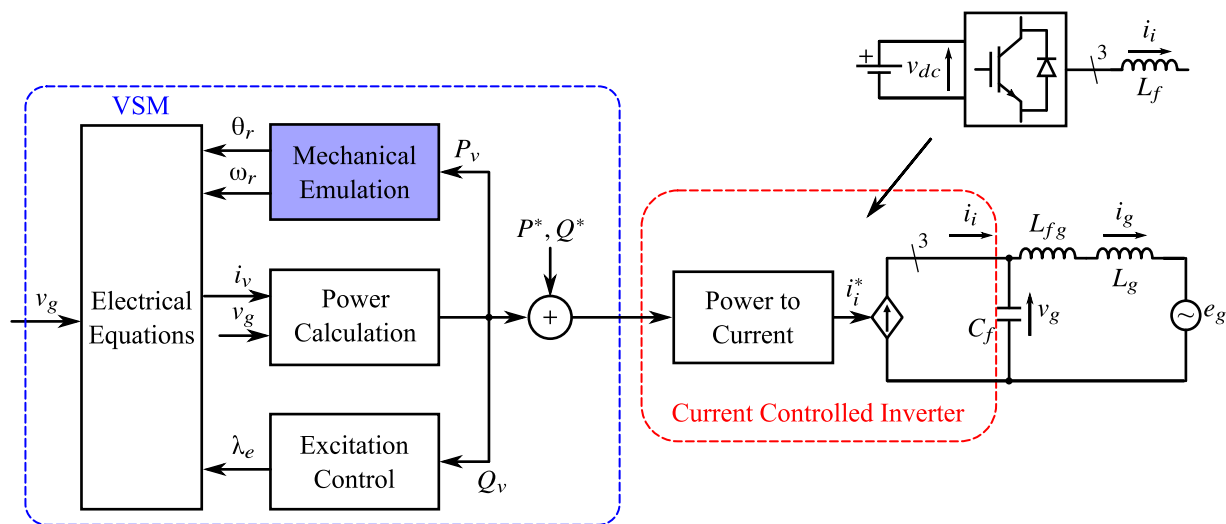
Fig. 1. Block diagram of the considered VSM controlling a grid-feeding inverter. The proposed lead-lag damping is implemented inside the mechanical emulation block (highlighted in blue).

droop control of conventional and VSM converters and it is not clear how to apply them in a VSM structure without droop control (e.g., conventional grid-following inverters enhanced with the provision of grid services).

To solve the drawbacks of conventional damping methods and the lead-lag based enhancements of droop controls, this paper proposes a simple damping method for VSMs based on a single lead-lag filter on its virtual power feedback. The proposed solution does not couple the damping and the active droop action (unlike droop-damping), does not require additional control parts (unlike PLL-damping) and does not require complex tuning or extra computational burden to the model. The proposed method is here applied to a VSM implementation available in the literature [16], but it can be easily extended to other models, being a filter on the feedback active power.

A second contribution of this paper is a general model to compare damping methods of VSMs and four performance indices. This method is presented and applied to highlight the benefits and drawbacks of the proposed solution with respect to the state of the art.

This paper is an extended version of [17]. The following modifications were performed to the original conference paper:

- Presentation of the discrete-time form of the proposed lead-lag damping, useful for hardware implementation;
- A novel generalized method to analyze and compare VSM damping techniques is included;
- Four performance indices to evaluate the various VSM damping methods are proposed and applied to compare five conventional damping strategies and the proposed one.

The proposed damping method is described in Section II along with its discrete-time formulation. Then, in Section III the tuning process of the proposed solution is described step-by-step. The conventional damping techniques against which the proposed one is compared are described in Section IV. Then, in Section V, a generalized method to analyze and

compare VSM damping techniques is presented along with four performance indices to compare VSM damping solutions. Finally, in Section VI the proposed solution is validated experimentally and compared to the conventional ones.

II. Lead-Lag Damping Description

The considered system is a VSM-driven current controlled inverter connected to the grid, as described in the block diagram of Fig. 1. The VSM generates the active and reactive power references P_v, Q_v to the inverter current controller [16]. The VSM is composed of the following functional blocks:

1) **Mechanical emulation** – this block emulates the mechanical behavior of the VSM, regulating the transfer of active power. This block generates both the active power reference P_v and the orientation of the current controller;
2) **Electrical equations** – this block implements the virtual stator of the VSM, receiving the measured grid voltage v_g across the filter capacitor C_f, the VSM speed ω_r and the virtual excitation flux linkage λ_e;
3) **Excitation control** – this regulates the exchange of reactive power [18];
4) **Power calculation** – calculates the virtual power of the VSM by multiplying its current i_v and the grid voltage v_g.

The proposed damping strategy only modifies the mechanical emulation block of the VSM. As shown in Fig. 2, the mechanical emulation is performed by implementing the well-known swing equation of SMs [4]. The term of the swing equation modeling the equivalent damping of the machine, proportional to the difference between the virtual speed ω_r and the rated grid speed ω_n is however excluded, as the damping is provided by the proposed lead-lag technique. Therefore, the mechanical emulation is simplified (see Fig. 2) and it is divided into two stages:
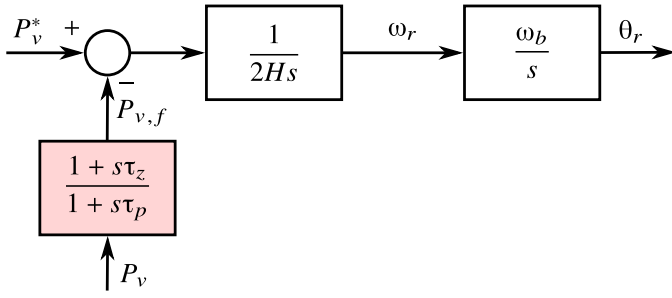
Fig. 2. Diagram of the mechanical emulation block with the proposed lead-lag damping (highlighted in red).

Fig. 3. Linearized model of the electromechanical part of the VSM using the proposed lead-lag damping.

1) Inertial part of the rotor, calculating the virtual rotor speed ω_r from the power error $P_v^* - P_{v,f}$, depending on the inertia constant H;
2) The rotor angle θ_r calculation from the virtual rotor speed ω_r (since the model is here expressed in per unit, it is necessary to define the base angular speed ω_b).

The proposed damping method modifies the mechanical emulation by adding a lead-lag filter on the feedback active power P_v of the VSM. The filtered active power $P_{v,f}$ is then fed to the rest of the mechanical emulation block, as depicted in Fig. 2. The proposed damping method is based on a lead-lag filter defined as

$$H_{LL}(s) = \frac{1 + s\tau_z}{1 + s\tau_p} \tag{1}$$

where the time constants of the pole τ_p and of the zero τ_z are the only two required parameters.

This damping solution can be implemented digitally by discretizing the $H_{LL}(s)$ transfer function. The resulting discrete-time expression of the lead-lag filter is as follows:

$$
\begin{aligned}
x_{LL}^{k+1} &= e^{-T_s/\tau_P} \cdot x_{LL}^k + (1 - e^{-T_s/\tau_P})\left(1 - \frac{\tau_z}{\tau_p}\right) \cdot P_v^k \\
P_{v,f}^k &= x_{LL}^k + \frac{\tau_z}{\tau_p} \cdot P_v^k
\end{aligned}
\tag{2}
$$

where T_s is the discretization time step, k is the discretization instant and x_{LL} is the internal state variable of the lead-lag filter.

III. PARAMETER TUNING

The two parameters of the proposed lead-lag filter τ_z and τ_p must be tuned in order to ensure the proper damping to the virtual machine. The two parameters τ_p and τ_z of the lead-lag filter are tuned based on the equivalent linearized model of the electromechanical part of the VSM, shown in Fig. 3. In this linearized model the interaction with the grid is modeled according to the traditional power system theory [4]. In particular, the following assumptions [19] are made:

1) The dynamic behavior of the inner current control loop is several orders of magnitude faster than the electromechanical part of the VSM. Therefore, it is simplified with a unity gain transfer function;
2) The virtual stator resistance is neglected, as it is much smaller than the stator and grid reactances in medium and high voltage grids;
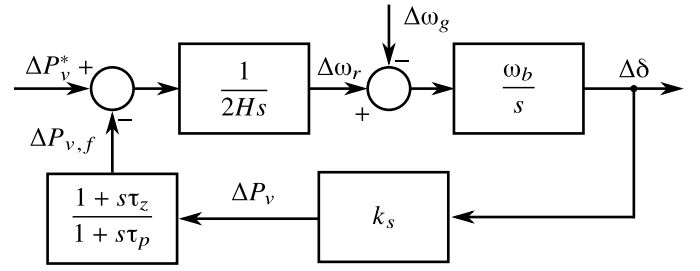
3) The virtual flux linkages of the VSM are considered constant in the first instants of the electromechanical transient [4];
4) The VSM is operating at no load, i.e., zero current, and nominal speed ($\omega_r = 1$ pu).

The active power exchange with the grid is therefore $\Delta P_v = k_s \Delta\delta$, where δ is the load angle of the VSM and k_s is the synchronizing power (maximum theoretical active power that can be exchanged with the grid). This power is defined as:

$$k_s = \frac{V_0 E_0}{X_s + X_g} \tag{3}$$

where X_s and X_g are the VSM and grid reactance, respectively, and V_0, E_0 are the grid voltage and the VSM back emf at the linearization point.

The characteristic equation of the linearized system of Fig. 3 can be derived as follows:

$$1 + \frac{1}{2Hs}\frac{\omega_b}{s}k_s\frac{1 + s\tau_z}{1 + s\tau_p} = 0 \tag{4}$$

Then, (4) can be rearranged to obtain the following:

$$s^3 + \frac{1}{\tau_p}s^2 + \frac{\omega_b k_s}{2H}\frac{\tau_z}{\tau_p}s + \frac{\omega_b k_s}{2H}\frac{1}{\tau_p} = 0 \tag{5}$$

and the variable a can be defined to simplify the notation:

$$a = \frac{\omega_b k_s}{2H} \tag{6}$$

To better analyze this linearized system, it is useful to compare (5) with a generic third order characteristic equation in the form:

$$(s^2 + 2\zeta\omega_0 s + \omega_0^2)(s + p_r) = 0 \tag{7}$$

This characteristic equation (7) features two complex poles defined by their damping ζ and natural frequency ω_0 and one real pole $-p_r$.

From (5), it emerges that the lead-lag filter parameters are tuned according to the desired electromechanical behavior of the VSM. The needed parameters, which must be provided by the user are the VSM inertia constant H, the synchronizing power k_s (i.e., information on the point of connection) and the desired damping coefficient ζ.

By comparing (5) and (7), the following relationships are found:

$$2\zeta\omega_0 + p_r \quad = \quad \frac{1}{\tau_p}$$

$$2\zeta\omega_0 p_r + \omega_0^2 \quad = \quad ak \qquad (8)$$

$$\frac{a}{\tau_p} \quad = \quad \omega_0^2 p_r$$

where $k = \tau_z/\tau_p$.

Having four variables (ω_0, p_r, k, τ_p) and only the three available relationships of (8), it is necessary to introduce an additional equation to uniquely derive the tuning parameters. A possible solution is to minimize the ratio $k = \tau_z/\tau_p$, which means reducing the high frequency gain of the lead-lag filter. This solution guarantees the least sensitivity from high frequency disturbances affecting the grid. Given that the damping coefficient ζ is a design input, it is possible to add the following condition:

$$\frac{\partial k}{\partial \omega_0} = 0 \qquad (9)$$

where the minimization depends only on ω_0.

From (8), it is possible to obtain p_r:

$$2\zeta\omega_0 p_r + \omega_0 \quad = \quad \omega_0 p_r \tau_p$$

$$p_r \quad = \quad \frac{\omega_0}{\omega_0\tau_p - 2\zeta} \qquad (10)$$

Then, by substituting (10) into (8):

$$2\zeta\omega_0 + \frac{\omega_0}{\omega_0\tau_p - 2\zeta} \quad = \quad \frac{1}{\tau_p}$$

$$2\zeta\omega_0\tau_z + \frac{\omega_0\tau_z}{\omega_0\tau_p - 2\zeta} \quad = \quad \frac{\tau_z}{\tau_p} = k \qquad (11)$$

The aforementioned minimization can be now applied to (11) as follows:

$$\frac{\partial k}{\partial \omega_0} \quad = \quad 0$$

$$2\zeta\tau_z + \frac{\tau_z(\omega_0\tau_p - 2\zeta) - \omega_0\tau_z\tau_p}{(\omega_0\tau_p - 2\zeta)^2} \quad = \quad 0$$

$$1 - \frac{1}{(\omega_0\tau_p - 2\zeta)^2} \quad = \quad 0 \qquad (12)$$

$$(\omega_0\tau_p - 2\zeta)^2 \quad = \quad 1$$

$$\omega_0\tau_p \quad = \quad 2\zeta \pm 1$$

Therefore, there are two solutions for $\omega_0\tau_p$, which can be used to derive p_r from (10):

$$\omega_0\tau_p \quad = \quad 2\zeta + 1 \quad \Rightarrow \quad p_r \quad = \quad \omega_0$$

$$\omega_0\tau_p \quad = \quad 2\zeta - 1 \quad \Rightarrow \quad p_r \quad = \quad -\omega_0 \qquad (13)$$

It is evident that the second solution ($\omega_0\tau_p = 2\zeta - 1$) is not acceptable, since it would lead to a real pole in the right half

plane for damping coefficient smaller than 1. It is therefore obtained that:

$$\omega_0^2 \quad = \quad (2\zeta + 1)a$$

$$p_r \quad = \quad \omega_0 \qquad (14)$$

$$k \quad = \quad (2\zeta + 1)^2$$

The final tuning values of the proposed lead-lag filter are as follows:

$$\tau_p \quad = \quad \sqrt{\frac{2H}{\omega_b k_s (2\zeta + 1)^3}}$$

$$\tau_z \quad = \quad \sqrt{\frac{2H}{\omega_b k_s}(2\zeta + 1)} \qquad (15)$$

IV. CONVENTIONAL DAMPING METHODS

The proposed solution is compared with the following conventional methods available in the technical literature:

1) **Droop-damping**: damping action proportional to the virtual speed error from nominal value;
2) **PLL-damping**: damping power proportional to the speed error from the measured grid frequency;
3) **PI-damping**: a proportional-integral (PI) regulator is used in place of the machine virtual rotor;
4) **Simplified virtual damper winding (RQ)**: the damper winding of SMs is modeled in a simplified way in the electrical equations of the VSM;
5) **High-Pass Droop-damping**: damping action proportional to the virtual speed error from nominal value filtered by a high-pass filter.

All these damping methods will be described and implemented in relative values (pu) for better comparison.

A. Droop-based Damping

The simplest solution available to provide electromechanical damping to a VSM is the droop-based damping and it is adopted by several models in the literature, such as [5], [15], [20]. This method implements the well known swing equation of synchronous generators [4]:

$$P_m - P_e = 2H\frac{d(\omega_r - \omega_g)}{dt} + D_p(\omega_r - \omega_g) \qquad (16)$$

imposing the grid frequency ω_g to its nominal value ω_n.

This means that the virtual speed ω_r and virtual rotor angle θ_r are calculated from the reference power P_v^* and the virtual feedback power P_v as follows:

$$2H\frac{d\omega_r}{dt} \quad = \quad P_v^* - (P_v + D_p(\omega_r - \omega_n))$$

$$\frac{d(\theta_r)}{dt} \quad = \quad \omega_r\omega_b \qquad (17)$$

The resulting block diagram is depicted in Fig. 4.

The tuning of this damping method is performed in a similar way as Section III, leading to the following damping coefficient D_p:

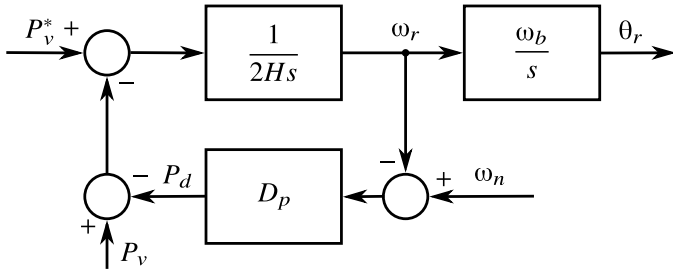$$D_p = 2\zeta\sqrt{2H\omega_b k_s} \qquad (18)$$

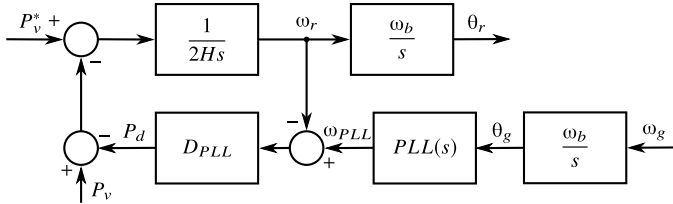Fig. 4. Diagram of the mechanical emulation block with the droop-based damping.

Fig. 5. Diagram of the mechanical emulation block with the PLL-based damping.

B. PLL-based Damping

A second common solution [6], [20], [21] is to use the grid frequency measured by a PLL instead of its nominal value. The implementation of this method is similar to the already presented droop-based damping. Here, (16) is modified and the measured grid frequency ω_{PLL} is used instead of its nominal value ω_n, as shown in Fig. 5.

The tuning procedure is equivalent to the one already presented in (18) for the droop-based damping. A correction coefficient is however necessary. This correction factor, depending on the machine and grid inductances, is obtained from empirical considerations and from the existing literature [6], [9] as follows:

$$D_{PLL} = D_p \cdot \frac{X_s + X_g}{X_s} = 2\zeta\sqrt{2H\omega_b k_s} \cdot \frac{X_s + X_g}{X_s} \quad (19)$$

C. PI-based Damping

The PI-based damping employs a PI regulator to eliminate the steady-state active power error of the VSM [15]. Therefore, the inertial block of the swing equation $(1/2Hs)$ is replaced by a PI regulator (see Fig. 6) defined as:

$$PI(s) = k_d + \frac{k_h}{s} \quad (20)$$

where k_d is the proportional term, providing damping, and k_h is the integral one, in charge of the inertial action.

The two parameters of the PI regulator k_d and k_h must be tuned in order to ensure the proper damping and inertia to the virtual machine. The tuning procedure is similar to the one of
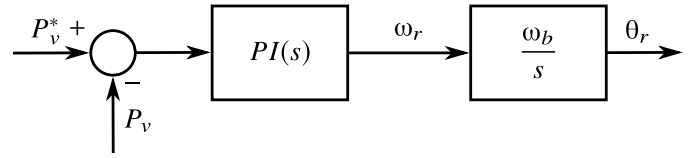

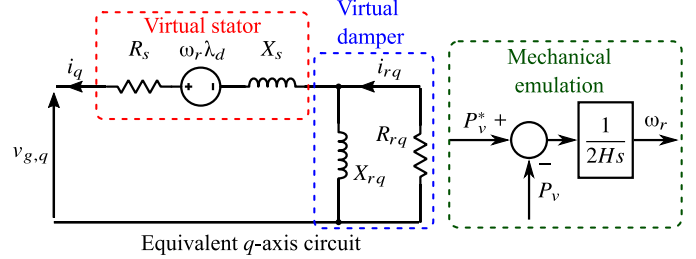Fig. 6. Diagram of the mechanical emulation block with the PI-based damping.

Fig. 7. RQ Damping: Electrical equation in the q-axis including the simplified virtual damper and relative mechanical emulation, featuring only inertia.

the droop-based and PLL-based and it leads to the following tuning values:

$$
\begin{aligned}
k_h &= \frac{1}{2H} \\
k_d &= 2\zeta\sqrt{\frac{k_h}{k_s\omega_b}}
\end{aligned}
\quad (21)
$$

D. RQ Damping

Another damping strategy here compared is the emulation of an SM damper winding [9], [22]. In this paper the q-axis simplified virtual damper [9] is considered and tuned according to [19]. This method is implemented in the electrical equations block of the VSM and the mechanical emulation only includes the inertia of the VSM with no damping. A summary of this strategy is shown in the diagram of Fig. 7, where the q-axis circuit of the VSM and its mechanical emulation are shown. The q-axis circuit acts similarly to a frequency-dependent impedance, which can be modeled as follows [19]:

$$Z_q(s) = X_g + X_{st}\frac{1 + s\tau_{rq}}{1 + s\tau_{rq0}} \quad (22)$$

where $X_{st} = X_s + X_{rq}$ is the sum of the VSM stator and damper reactances and $\tau_{rq} = s\tau_{rq0}\frac{X_s}{X_{st}}$ is the short circuit time constant of the VSM. τ_{rq0} is the open circuit time constant of the VSM [19].

E. High-Pass Droop-based Damping

The last damping strategy is an improvement of the droop-based damping. This method filters the damping power term using an high-pass (HP) filter as in (23) in series with the damping gain D_p. The resulting block diagram is depicted in Fig. 8.

The tuning of this damping method is performed as for the droop-based damping shown in Section III, using the
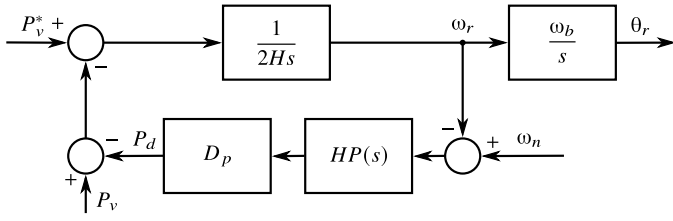
Fig. 8. Diagram of the mechanical emulation block with the High-Pass droop-based damping.

same damping coefficient D_p and a time constant τ_{HP} of the filter, selected according to the range of frequency oscillations that must be damped by the VSM (ranging up to the sub-synchronous oscillations in the range of 1-5 Hz) [23].

$$HP(s) = \frac{s \cdot \tau_{HP}}{s \cdot \tau_{HP} + 1} \qquad (23)$$

V. DAMPING PERFORMANCE INDICES AND SCHEMATIC BLOCK FOR DAMPING COMPARISON

To fairly compare the various damping strategies, a unique linearized model is developed and then studied by means of transfer functions. A performance index will be related to each of these transfer functions.

To begin, the linearized model is based on the following assumptions, deriving from the classical theory of power system analysis (i.e., Heffron Phillips model [4], [24]):

1) The virtual resistance of the VSM is neglected (i.e., $R_s = 0$);
2) The virtual flux linkages are assumed to be constant in the first instants of the electromechanical small signal transient. Therefore,

$$\frac{d\lambda_d}{dt} = \frac{d\lambda_q}{dt} = \frac{d\lambda_e}{dt} = 0; \qquad (24)$$

3) The VSM is operating at no load, i.e., $P_0 = Q_0 = 0$ and so are the virtual currents of the machine;
4) The linearization is performed around the nominal grid frequency $\omega_r = 1$ pu. This is true for the small signal analysis of the damping techniques, implemented on VSMs operating normally at the rated grid frequency;
5) The behavior of the internal controller is considered to be orders of magnitude faster (kHz) than the electromechanical transients (few Hz) and it is therefore approximated to a unity gain transfer function.

Under these assumptions, the VSM and grid system can be modeled by the following linearized system, shown in Fig. 9.

This linearized model is presented in the most general way, so that it can be applied to each presented damping method, by simply modifying the following fundamental blocks:

- **Mechanical block** $M(s)$ describing the virtual mechanical emulation of the VSM, relating the active power error and the virtual speed;
- **Electrical emulation and grid block** $E(s)$ describing the virtual stator of the VSM and its interaction with the grid;
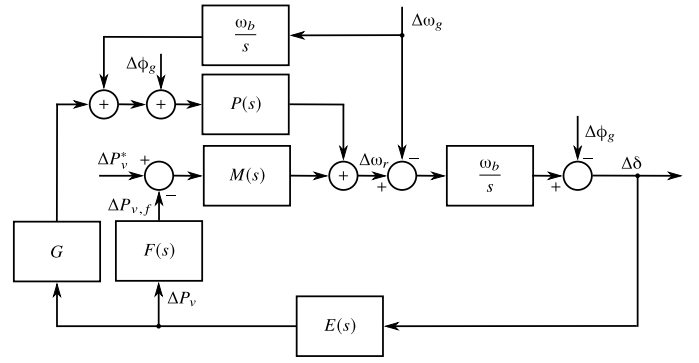

Fig. 9. Block diagram of the linearized electromechanical model of VSMs for damping comparison.

TABLE I
TRANSFER FUNCTIONS OF THE LINEARIZED MODEL FOR EACH DAMPING SOLUTION.

Method	$M(s)$	$E(s)$	$F(s)$	$P(s)$	G
Droop	$\dfrac{1}{2Hs + D_p}$	k_s	1	0	0
PLL	$\dfrac{1}{2Hs + D_{PLL}}$	k_s	1	$\dfrac{PLL(s)D_{PLL}}{2Hs + D_{PLL}}$	$\dfrac{X_g}{V_0^2}$
PI	$k_d + \dfrac{k_h}{s}$	k_s	1	0	0
RQ	$\dfrac{1}{2Hs}$	$\dfrac{E_0 V_0}{Z_q(s)}$	1	0	0
LL	$\dfrac{1}{2Hs}$	k_s	$\dfrac{1 + s\tau_z}{1 + s\tau_p}$	0	0
HP	$\dfrac{1}{2Hs + D_p HP(s)}$	k_s	1	0	0

- **Grid frequency estimation block** effect on the VSM $P(s)$, to include and describe the action of the PLL (if any);
- **Filter** on the active power feedback $F(s)$;
- **Effect** of the power on the angle measured by the PLL $G(s)$, where:

$$G(s) = \begin{cases} k_g = \dfrac{X_g}{V_0^2} & \text{PLL-based} \\ \\ 0 & \text{Other solutions} \end{cases} \qquad (25)$$

These blocks assume different values for each damping method. Table I summarizes the values of each block for the considered damping methods.

To study the effect of the different disturbances that may occur from the grid side, the following inputs are introduced:

- Grid frequency variation $\Delta\omega_g$;
- Phase jumps of the grid voltage $\Delta\phi_g$, occurring during short circuits in the grid [25];
- Active power reference variation ΔP_v^*, emulating an active power setpoint variation of the generating unit.

Finally, the following indices are proposed to evaluate the performance of the damping strategies. These indices consist of transfer functions that describe specific behaviors of the VSM and that can be quantitatively used to compare damping

solutions by means of the initial and final value theorems, as it will be explained later.

- **Embedded active droop action**: this quantifies how much active power is injected by the VSM when it is operating at non-nominal grid frequency. Transfer function $\Delta P_v/\Delta\omega_g$;
- **Inertial effect**. Active power injection in case of a grid frequency variation (frequency derivative). Transfer function $\Delta P_v/s\Delta\omega_g$;
- **Sensitivity** of the **virtual rotor speed** ω_r to grid disturbances (such as phase jumps). Transfer function $\Delta\omega_r/\Delta\phi_g$;
- **Step response** to the active power reference variation. Transfer function $\Delta P_v/\Delta P_v^*$.

In the following subsections, each of these indices will be explained and justified. Besides, the five considered damping methods will be compared theoretically considering a VSM with the following specifications: $\omega_b = 2\pi \cdot 50$ rad/s; $H = 4$ s (value in the range of inertia constants of SMs); $\zeta = 0.7$ (good damping); $k_s = 5$ pu (grid working at nominal voltage and relatively stiff); $X_s = X_g = 0.1$ pu (relatively stiff grid and stator inductance compatible with the subtransient inductances of SMs); PLL bandwidth set to 20 Hz; the cut-off frequency of the high-pass filter set to 0.16 Hz and thus a time constant as follows

$$\tau_{HP} = \frac{1}{2\pi \cdot 0.16 \text{ Hz}} = 1 \text{ s} \tag{26}$$

The selected frequency of 0.16 Hz is motivated by the range of frequency oscillations that must be damped by the VSM (ranging up to the sub-synchronous oscillations in the range of 1-5 Hz) and it is corroborated by the literature [11], [23].

A. Embedded active droop action

The first comparison index we propose is the embedded active droop action. In many VSM models, the traditional swing equation of SMs [4] is implemented in the mechanical emulation block (such as for the droop-based damping). This equation is as follows:

$$P_v^* - P_v = 2H\frac{d(\omega_r - \omega_g)}{dt} + D_P(\omega_r - \omega_g) \tag{27}$$

Even though this equation is valid and useful for power systems representations, it leads to some practical problems in the actual implementation of VSMs. In fact, in many VSM implementations, the damping term depends on the difference between the virtual rotor speed ω_r and the reference grid speed ω_g^* (i.e., $D_P(\omega_r - \omega_g^*)$). This introduces a strong active droop effect in case the actual grid frequency ω_g (and therefore ω_r) is different from its reference value ω_g^*. It can be proven [9], [20], [26], [27] that the necessary damping coefficient D_P (calculated by (18)) is around an order of magnitude larger than the usual droop controller gains. This would lead to an abnormal active power injection from the VSM, in case the grid frequency is slightly different from its reference value.
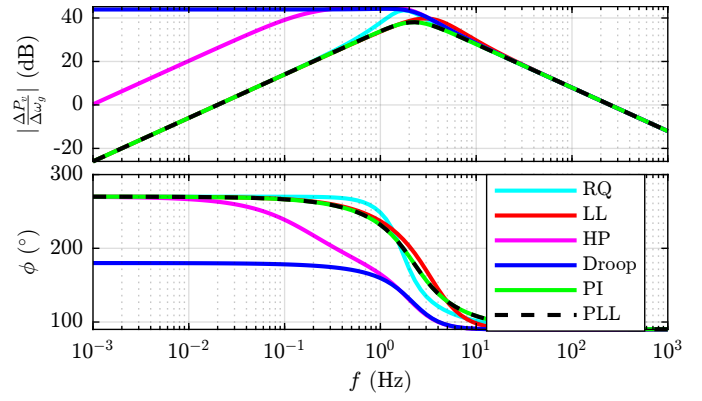

Fig. 10. Transfer functions of the embedded droop characteristic of the VSM with the considered damping methods.

It is therefore important to quantify this coupling with the following transfer function:

$$\frac{\Delta P_v}{\Delta\omega_g}(s) = \left(\frac{\omega_b}{s}P(s) - 1\right)\frac{E(s)\omega_b}{s + E(s)\omega_b[F(s)M(s) - G(s)P(s)]} \tag{28}$$

Ideally, the VSM should not have any embedded non-tunable droop effect. This means:

$$\left.\frac{\Delta P_v}{\Delta\omega_g}\right|_{s\to 0} = 0 \tag{29}$$

By replacing the values of Table I in (28) for each damping method, the Bode diagrams of Fig. 10 are plotted. The explicit transfer functions are provided in the Appendix for all the considered methods.

It can be easily calculated, and seen graphically in Fig. 10, the active power injected by each damping method when the grid is operating at non-nominal frequency at steady-state ($s \to 0$):

$$\left.\frac{\Delta P_v}{\Delta\omega_g}\right|_{s\to 0} = \begin{cases} D_P & \text{Droop-based} \\ \\ 0 & \text{Other solutions} \end{cases} \tag{30}$$

Therefore, the droop-based damping will inject active power into the grid when the grid frequency is different from its nominal value (e.g., frequency after a fault, before the action of primary and secondary frequency control). The amount of injected active power depends on the value of the damping coefficient D_P. This would not represent an issue, if the damping coefficient D_P were equal or similar to traditional active droop coefficients (around 2% to 5% [4]). However, according to (18), $D_P = 157$ pu. This value is around ten times larger that the usual droop coefficients (5–20 pu). Therefore, the active power injected is around ten times larger than the one expected by the typical primary regulation of the frequency.

This is not the case with the other methods, as their low frequency gain is 0. Therefore, if the grid frequency is different from its nominal value, they will not inject any active power into the grid. If a primary frequency regulation logic is needed, an external droop controller can be added. This droop
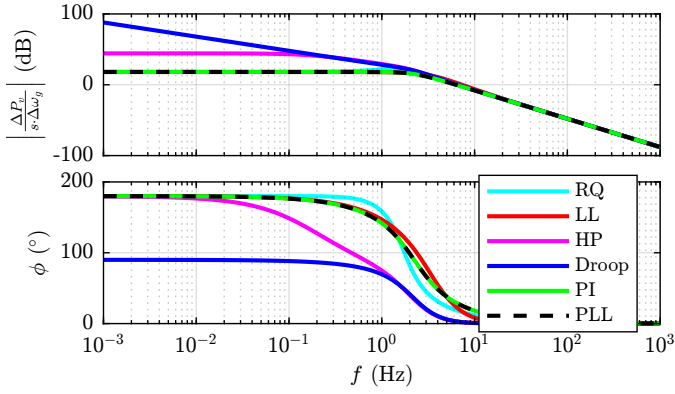
Fig. 11. Transfer functions of the inertial effect of the VSM with the considered damping methods.

controller can be freely tuned, according to the usual droop coefficients.

B. Inertial Effect

A core function of VSMs is the so-called synthetic inertia [2]. This means that the VSM must inject active power proportional to the derivative of the grid frequency f_g and its inertia constant H:

$$P_{inertial} = -2H\frac{df_g}{dt} \qquad (31)$$

This function is crucial in the context of high penetration of renewable energy sources into the electric grid. In fact, when the electric power system lacks of mechanical inertia (phasing out synchronous machines, e.g., of coal power plants), the rate of change of frequency (ROCOF) during load/generation transients can increase beyond the admissible levels (protection devices thresholds). An inertial power injection from grid connected electronic converters represents therefore a valid solution to this issue.

As the inertial power injection is inversely proportional to the derivative of the grid frequency, the following transfer function must be analyzed to study the inertial effect of a VSM:

$$\frac{\Delta P_v}{s\Delta\omega_g}(s) = \frac{1}{s}\left(\frac{\omega_b}{s}P(s) - 1\right)\frac{E(s)\omega_b}{s + E(s)\omega_b[F(s)M(s) - G(s)P(s)]} \qquad (32)$$

Therefore, it is desirable that:

$$\left.\frac{\Delta P_v}{s\Delta\omega_g}\right|_{s\to0} = 2H \qquad \angle\left.\frac{\Delta P}{s\Delta\omega_g}\right|_{s\to0} = 180° \qquad (33)$$

representing the amplitude of the inertial support and its counteracting effect against frequency variations.

Similarly to what was done in the previous subsection, the blocks of Table I are replaced in (32), resulting to the Bode plots of Fig. 11. The explicit transfer functions are provided in the Appendix for all the considered methods.

The active power injected by each damping method when the grid frequency varies linearly ($s \to 0$) is:

$$\left.\frac{\Delta P_v}{s\Delta\omega_g}\right|_{s\to0} = \begin{cases} \infty\angle90° & \text{Droop-based} \\[2mm] (2H + D_P\tau_{HP})\angle180° & \text{HP-damping} \\[2mm] 2H\angle180° & \text{Other solutions} \end{cases} \qquad (34)$$

It is therefore evident how the droop-based damping will inject a far too large active power when counteracting frequency variations, while the RQ, LL, PI and PLL damping methods comply with the inertial requirements. Finally, the HP damping method shows an inertial effect which is a function not only of the inertia constant H, but even of the damping constant and the cut-off frequency of the high-pass filter. This results in a too large active power injection, as the equivalent inertial contribution is about twenty times larger than the desired one:

$$\frac{2H + D_P\tau_{HP}}{2H} = \frac{164.11}{8} = 20.51 \qquad (35)$$

The droop-based and the HP damping methods behaviors are more like a fast primary frequency control, rather than a VSM providing virtual inertia. At grid level, this behavior is not necessarily negative (it still supports the grid frequency). However, this is a serious drawback when sizing the dc side of the VSM converter. The dc side must in fact be able to provide larger active power and energy even during short frequency variation, even though the inverter unit is not intended to take part to the primary regulation of the frequency (e.g., small rated power).

C. Sensitivity to Phase Jumps During Faults

An often neglected aspect of VSMs is that a good estimation of the actual grid frequency by means of the virtual rotor speed is desirable. This measurement can be in fact used for grid monitoring and/or protection. To this purpose, it is important that the virtual rotor speed ω_r is affected as little as possible by grid voltage variations. A first source of disturbances is the phase jump $\Delta\phi_g$ of the grid voltage vector during faults [25]. The transfer function which can be used to quantify this effect is as follows:

$$\frac{\Delta\omega_r}{\Delta\phi_g} = \frac{s[P(s) + F(s)E(s)M(s) - G(s)E(s)P(s)]}{s + E(s)\omega_b[F(s)M(s) - G(s)P(s)]} \qquad (36)$$

The goal in this case is that the VSM is as little as possible sensitive to phase jumps $\Delta\phi_g$ of the grid voltage vector. This means that:

$$\left.\frac{\Delta\omega_r}{\Delta\phi_g}\right|_{s\to\infty} = 0 \qquad (37)$$

As done before, by replacing the values of Table I in (36) for each damping method, the Bode diagrams of Fig. 12 are obtained. The explicit transfer functions are provided in the Appendix for all the considered methods.

It is evident from Fig. 12 that both the PLL-based and the PI-based damping methods are more sensitive to phase jumps of the grid voltage vector. On the other hand, the other four damping methods (Droop-based, RQ, lead-lag and HP) are
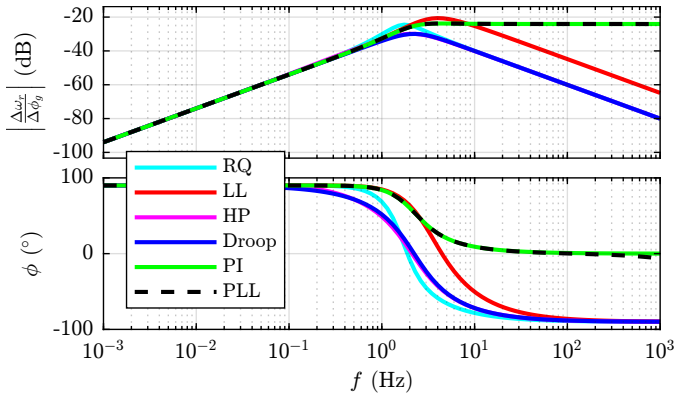
This article has been accepted for publication in IEEE Transactions on Industry Applications. This is the author's version which has not been fully edited and content may change prior to final publication. Citation information: DOI 10.1109/TIA.2023.3293779

9

Fig. 12. Transfer functions of the sensitivity of the VSM to phase jumps with the considered damping methods.

Fig. 13. Transfer functions of the active power reference tracking of the VSM with the considered damping methods.

more immune to such disturbances. Therefore, when using these four damping methods the virtual speed ω_r represents a more valid estimation of the actual grid frequency and can be used for monitoring and protection functions.

D. Step response to the active power reference variation

Finally, the fourth comparison index is the step response to the active power reference variation. It replicates, for instance, the change in the active power generation of the dc source of the VSM (e.g., change of the power produced by a PV plant or a wind turbine). The transfer function needed to study the step response is the following:

$$\frac{\Delta P_v}{\Delta P_v^*} = \frac{\omega_b E(s) M(s)}{s + E(s)\omega_b [F(s)M(s) - G(s)P(s)]} \quad (38)$$

This transfer function must guarantee zero steady-state tracking error when a constant reference is given. Therefore, it is necessary that:

$$\left.\frac{\Delta P_v}{\Delta P_v^*}\right|_{s\to 0} = 0 \qquad \left.\angle\frac{\Delta P}{\Delta P_v^*}\right|_{s\to 0} = 0° \quad (39)$$

As for the previous performance indices, by replacing the values of Table I in (38) for each damping method, the Bode diagrams of Fig. 13 are retrieved. The Appendix provides the explicit transfer functions for all the considered methods.

It can be observed from Fig. 13 that each damping method shows both zero gain and zero phase. Therefore, power reference tracking with no error is expected for each solution. Moreover, it is expected that the PI-based damping will feature the fastest dynamic behavior, being its gain larger on the whole frequency range. On the other hand, it is expected that the RQ-damping will have an under damped behavior with larger overshoot. More quantitative results can be obtained numerically from the poles of the transfer function (38).

VI. EXPERIMENTAL VALIDATION

A 15 kVA two-level three-phase inverter, controlled at 10 kHz by a dSPACE 1005 platform, has been used for experimental validation. The experimental setup is diagrammed in Fig. 14 and depicted in Fig. 15. This inverter is connected to a grid emulator (rated 50 kVA and emulating a 120 Vrms
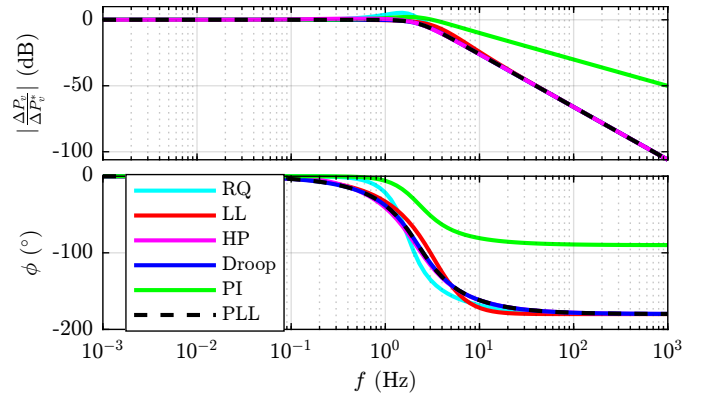
phase voltage grid at 50 Hz) through an LCL filter (L_f = 545 μH, C_f = 22 μF and L_{fg} = 120 μH). An equivalent grid impedance of L_g = 300 μH is placed between the inverter and the grid emulator.

The proposed method has been validated against five conventional methods available in the literature and described in Section IV: Droop-damping, PLL-damping, PI-damping, RQ-damping and High-Pass Droop-damping. To ensure a fair comparison, the tuning of all methods was performed using the same inputs (H = 4 s, ζ = 0.7 and k_s = 5 pu).

Five tests were carried out:

1) Grid frequency drop after a major power imbalance. This test checks the coupling between the damping action and the active droop action. If the response is decoupled, no active power is injected after the frequency transient;
2) Inertial response of the VSM. This test evaluates the inertial power injection of the VSM by applying a triangular frequency variation (0.2 Hz peak-peak with 2 s period). The VSM should inject an active power equal to $2H \cdot \Delta f / \Delta t$, with $\Delta f / \Delta t$ = 0.2 Hz/s;
3) Voltage dip with phase displacement (−2% voltage and −2° phase jump). This tests the quality of the virtual speed in case of grid disturbances. The smaller the speed variation, the better the rejection. Only a voltage dip was tested, but the same applies for swells, as the model reacts to small signal variations in a symmetrical way.
4) Step variation of the active power reference from 0.1 pu to 0.3 pu. This test checks the response of the VSM in case of a variation of the active power reference step (e.g., emulating the power setpoint change of a renewable power plant) for the considered damping methods of the paper.
5) V-curve of the proposed lead-lag damping, showing the reactive power-excitation flux linkage (Q_i, λ_e) relationship to demonstrate that there is no adverse influence on the reactive behavior at steady-state.

A. Test 1: Grid Frequency Drop

In Test 1 (see Fig. 16) a major power imbalance in the grid is emulated. The grid frequency drops to a nadir of 49.2 Hz and then settles to a final value of 49.75 Hz. The magnitude
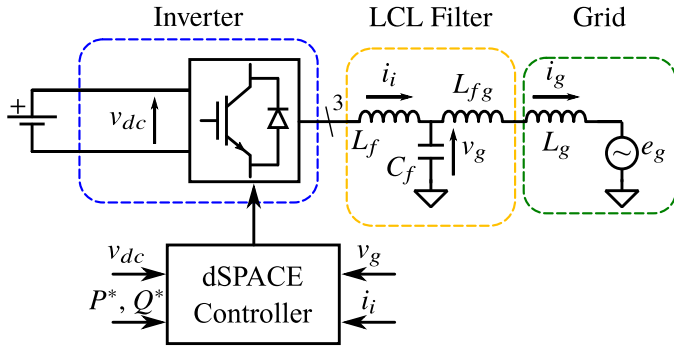
This article has been accepted for publication in IEEE Transactions on Industry Applications. This is the author's version which has not been fully edited and content may change prior to final publication. Citation information: DOI 10.1109/TIA.2023.3293779

10

Fig. 14. Block diagram of the experimental setup.

Fig. 15. Picture of the experimental setup.

Fig. 16. Test 1. Grid active power imbalance. The response of the proposed lead-lag damping (LL) against five conventional methods is presented in terms of virtual speed ω_r and active power injection P_i into the grid.
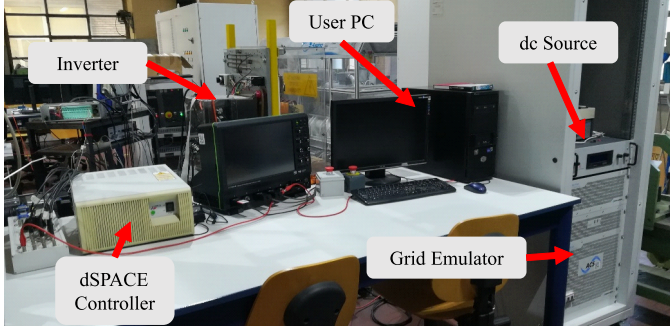
of the emulated imbalance has been amplified with respect to actual grid fluctuations to highlight the differences between the damping methods. For a fair comparison, an external frequency droop controller (droop gain 5% [4]) was implemented. Each compared method tracks the grid frequency with no oscillations. However, the droop-damping almost immediately saturates the active power injection to the inverter current limit set to 0.6 pu. This unwanted too large power injection is due to the necessary damping gain of the droop-damping (around 10 times larger than standard droop coefficients). The PLL-based, PI-based, RQ and the proposed LL methods feature an inertial behavior in the early phase of the transient and later a proportional regulation of the frequency with a power injection compliant with the designed droop controller. They inject inertial power and active droop power during all the transient. However, in this case, the droop power injection is limited and complies with the design droop coefficient (i.e., an active power when the frequency stabilizes equal to 0.1 pu). As regards the HP damping method, in the early stage of the transient it behaves like the droop-damping solution. Indeed, the large damping gain D_P leads to the immediate injection of a large amount of active power, up to the saturation limit. However, in steady-state, the damping contribution is zero because of the high-pass filter implementation. Therefore, the HP damping solution transiently contributes with a proportional regulation of the frequency, for a duration depending on the time constant of the high pass filter (around 5 times τ_{HP}). In conclusion, the droop-based damping is much inferior compared to the other damping methods, as it injects a too large active power when the grid frequency is far from its
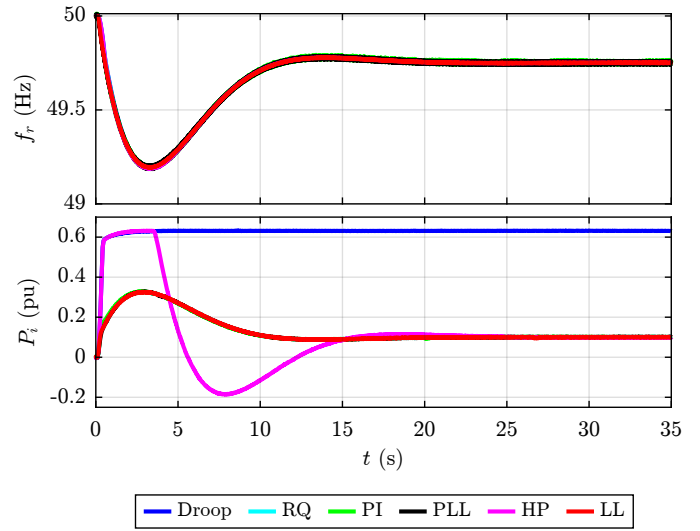
rated value. The other damping methods are equivalent under this aspect.

B. Test 2: Inertial effect

To evaluate the inertial response of the VSM, it is useful to impose a linear variation of the grid frequency. Therefore, during the second test a triangular grid frequency variation was applied with a peak-peak value of 0.2 Hz and a period of 2 s. The expected VSM response is an active power injection proportional to the frequency derivative according to the following:

$$P_v = 2H \cdot \frac{\Delta f}{\Delta t} = 2 \cdot 4 \text{ s} \cdot \frac{0.2 \text{ Hz}}{50 \text{ Hz} \cdot 1 \text{ s}} \text{ pu} = 0.032 \text{ pu} \quad (40)$$

Being the frequency triangular, the expected power injection should be a squarewave, with amplitude 0.032 pu and period 2 s. As it can be noticed from the results of Fig. 17, four of the considered damping strategies (PI-based, PLL-based, RQ and the proposed LL damping) inject the correct amount of active power with the correct shape, therefore contributing to reduce the grid frequency derivative. On the other hand, the droop-based and the HP damping methods hide the inertial effect behind a strong proportional frequency regulation, leading to a triangular power injection with an amplitude around 10 times larger than the expected 0.032 pu. As stated for the previous test, this aspect is not necessarily negative for the grid frequency quality, as it acts as a fast frequency regulation. However, this can represent a drawback when designing the dc side of the converter. According to the desired operation (only inertia or inertia and frequency regulation), the dc supply must be sized to provide the energy and power during the frequency transient. In case of true inertial behavior (PI-based, PLL-based, RQ and the proposed LL damping), this energy swing is quite limited, as it can be seen in the bottom plot of Fig. 17. On the other hand, the droop-based damping and HP damping feature an energy variation roughly 5 times larger (primary
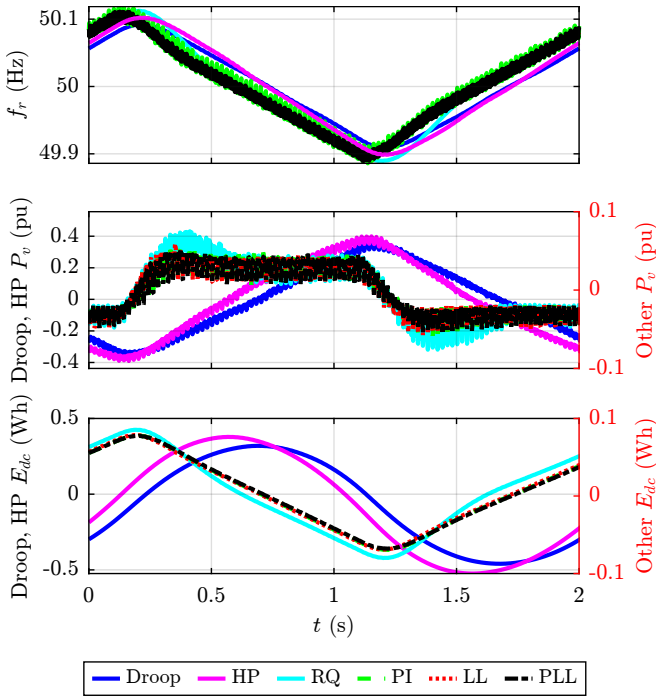
This article has been accepted for publication in IEEE Transactions on Industry Applications. This is the author's version which has not been fully edited and content may change prior to final publication. Citation information: DOI 10.1109/TIA.2023.3293779

11

Fig. 17. Test 2. Inertial effect comparison. The active power injection P_v and the dc energy fluctuation E_{dc} are shown when the grid frequency varies between 49.9 and 51.1 Hz. The vertical axes of the power and energy are distinguished according to the damping method. The Droop-damping and HP-damping are linked to the left axis, the others to the right axis.

frequency regulation), thus forcing the converter designer to increase the storage capacity of the converter (supercapacitor banks or batteries), thus increasing the complexity and the cost of the conversion system.

C. Test 3: Voltage Dip

In Test 3 (see Fig. 18), the VSM was perturbed by an emulated −2% voltage dip with a −2° phase jump. The magnitude of the perturbation was chosen in order to avoid the current limitation of the converter during this test. Since this test verifies the limited sensitivity of the proposed damping method against disturbances, the virtual speed ω_r of the VSM was compared for each considered damping method. In this matter, the droop-damping and the HP damping are superior, since they show the least sensitivity of the virtual speed to grid disturbances. The other four methods (PLL-based, PI-based, RQ and LL) are more sensitive to grid disturbances, leading to larger virtual speed deviations. In particular, the PI-based shows the largest speed variation (−125 mHz) and the largest steady-state high frequency oscillations, caused by the current and voltage measurement noise. This large variation in the first instants of the perturbation is due to the direct feed-through (related to the proportional term k_d) from the active power feedback to the virtual speed ω_r. Better results, with slightly lower sensitivity, are obtained with the PLL-based and LL-damping. In this case, the proposed LL-damping is not the best, but represents a good compromise between the solutions, featuring a reduced speed deviation during the perturbation.
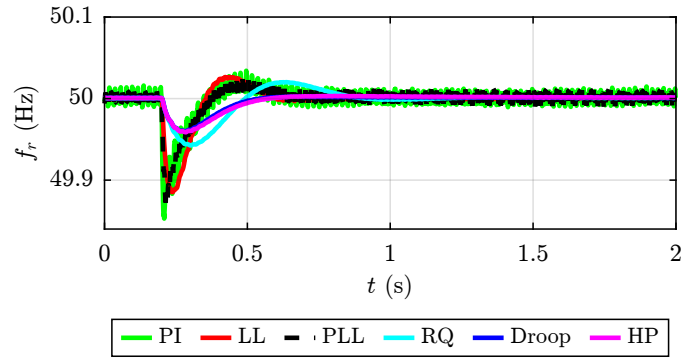

Fig. 18. Test 3. Voltage dip. The virtual speed sensitivity to grid disturbances is validated with a −2% voltage dip and −2° phase jump. The responses of the conventional and proposed LL damping techniques are compared in terms of virtual speed f_r variations.
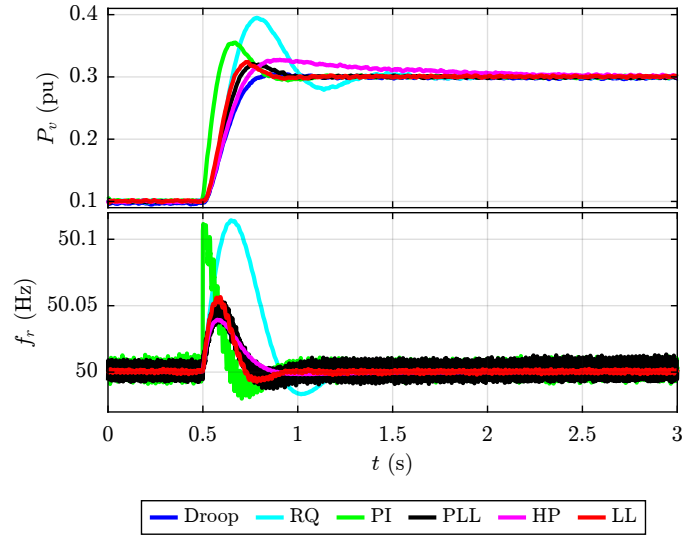

Fig. 19. Test 4. Step response of the VSM against an active power reference variation from 0.1 pu to 0.3 pu.

D. Test 4: Active power step variation

In Test 4 (see Fig. 19), the active power reference of the VSM is changed from 0.1 pu to 0.3 pu, by emulating, for instance, a change of the power produced by renewable power source at the dc-side. In the experiment, the active power output P_v and the frequency f_r of the VSM virtual rotor are shown. As it already emerged from the theoretical analysis of Section V, the VSM is able to track correctly the active power reference at steady state. The PI-damping features the fastest rising time (as it emerged from the Bode diagram of Fig. 13). However, this comes at the price of a significant overshoot of 0.05 pu. The RQ-damping is clearly the worst performing in terms of overshoot (0.1 pu). On the other hand, the other damping methods (including the proposed LL-damping) show very similar trends, with limited overshoot and satisfactory settling times.

E. Test 5: V-curve

To demonstrate that the reactive power exchange does not depend on the damping technique, we experimentally obtained

TABLE II
SUMMARY OF THE COMPARED DAMPING METHODS FOR VSMs.

| Feature	Droop	PLL	PI	RQ	LL	HP
Parameters	D_p	D_{PLL}	k_d, k_h	L_{rq}, τ_{rq0}	τ_z, τ_p	D_p, τ_{HP}
Implementation	Very simple	Complex	Simple	Average	Average	Simple
Embedded droop (Test 1)	Yes	No	No	No	No	Transiently
Inertial effect (Test 2)	Too large	Ok	Ok	Ok	Ok	Too large
Disturbance Rejection (Test 3)	Best	Average	Worst	Good	Average	Best
Step Response (Test 4)	Best	Good	Average	Worst	Good	Average
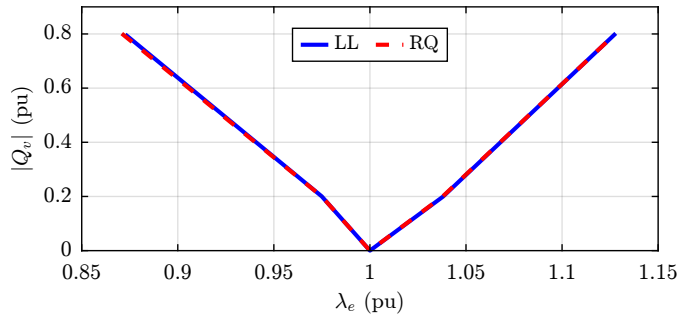
Fig. 20. Test 5. V-curve of the virtual synchronous machine showing the relationship between the excitation flux linkage and reactive power injection.

the reactive power curve as a function of the excitation flux linkage for the nominal grid voltage. The result is shown in Fig. 20 for the proposed lead-lag damping and RQ. As it can be seen in the figure, the VSM is able to adjust its excitation to regulate the reactive power exchange. The magnitude of the excitation flux linkage variation depends on the chosen virtual stator inductance L_s and the grid inductance L_g. In this experimental test, we had $L_s = 0.1$ pu and $L_g = 0.05$ pu. As it can be noticed, for a reactive power of 0.8 pu, the flux linkage variation well corresponds to the theoretical analysis of (41).

$$\Delta\lambda_e = \Delta Q_v \cdot (L_s + L_{fg} + L_g) = 0.8 \cdot 0.17 = 0.136 \text{pu} \quad (41)$$

F. Summary of Damping Methods

Table II summarizes the presented damping strategies to highlight their key differences. The comparison is carried out in terms of number of parameters needed by the damping method, easiness of implementation and the five benchmark experimental tests. From this summary comparison is clear that the proposed lead-lag technique represents a viable solution for the VSMs electromechanical damping, compared to conventional ones.

VII. CONCLUSION

The smooth integration of RESs into the electric grid will require advanced control techniques for power electronics converters. To this purpose, a viable solution is the concept of VSM, which is capable of emulating and even outperforming traditional SMs. To obtain the best performance from VSMs, it is necessary to implement a correct electromechanical damping strategy. This way, the speed and power oscillations of the VSM are limited and the VSM-controlled inverter is enabled to damp low frequency oscillations in the power system. In this paper a damping solution for VSMs has been proposed and described. The proposed method consists of a single lead-lag filter on the active power feedback of VSMs, therefore representing a simple and straightforward solution with respect to most of the existing damping techniques available in the literature. Its performance was then validated experimentally and compared against five conventional damping methods for VSMs, leading to the summary comparison of Table II. This comparison is based on the four performance indices proposed in this paper, which test important features of damping methods: embedded droop action, inertial effect, sensitivity to phase jumps in the grid voltage and step response to an active power reference variation. From this comparison, it emerges that the proposed lead-lag damping satisfies the requirement of full decoupling between the damping of the VSM and the frequency droop action of the plant, differently from the conventional droop-based damping. On top of that, the proposed lead-lag damping is able to provide the correct amount of inertial active power during frequency variations, without burdening the dc converter supply with unnecessary frequency droop effect. Moreover, the proposed method also features high rejection of any faulty condition in the grid voltage, limiting the sensitivity of the VSM virtual speed against disturbances.

APPENDIX

In this appendix the performance indices transfer functions are presented for each of the five considered damping solutions.

This article has been accepted for publication in IEEE Transactions on Industry Applications. This is the author's version which has not been fully edited and content may change prior to final publication. Citation information: DOI 10.1109/TIA.2023.3293779

13

Embedded active droop action

$$\frac{\Delta P_v}{\Delta \omega_g} =$$

$$\begin{cases} -\dfrac{2Hk_s\omega_b s + D_p k_s \omega_b}{2Hs^2 + D_p s + k_s \omega_b} & \text{Droop} \\[3mm] -\dfrac{\omega_b k_s \left(2Hs^2 + D_{PLL}s - PLL(s)D_{PLL}\omega_b\right)}{2Hs^3 + D_{PLL}s^2 + k_s \omega_b \left(1 - k_g PLL(s)D_{PLL}\right)} & \text{PLL} \\[3mm] -\dfrac{2HE_0V_0\omega_b s}{2HZ_q s^2 + E_0 V_0 \omega_b} & \text{RQ} \\[3mm] -\dfrac{k_s \omega_b s}{s^2 + (k_d s + k_h)\,\omega_b k_s} & \text{PI} \\[3mm] -\dfrac{2H\omega_b k_s \left(1 + s\tau_p\right) s}{2H\left(1 + s\tau_p\right)s^2 + \omega_b k_s \left(1 + s\tau_z\right)} & \text{LL} \\[3mm] -\dfrac{2Hk_s\omega_b s + D_p HP(s) k_s \omega_b}{2Hs^2 + D_p HP(s)s + k_s \omega_b} & \text{HP} \end{cases}$$

$$(42)$$

Sensitivity to Phase Jumps During Faults

$$\frac{\Delta \omega_r}{\Delta \phi_g} =$$

$$\begin{cases} \dfrac{k_s s}{2Hs^2 + D_p s + k_s \omega_b} & \text{Droop} \\[3mm] \dfrac{k_s s + sPLL(s)D_{PLL}\left(1 - k_g k_s\right)}{2Hs^2 + D_{PLL}s + k_s \omega_b (1 - k_g PLL(s)D_{PLL})} & \text{PLL} \\[3mm] \dfrac{E_0 V_0 s}{2HZ_q s^2 + E_0 V_0 \omega_b} & \text{RQ} \\[3mm] \dfrac{k_s \left(k_d s + k_h\right) s}{s^2 + (k_d s + k_h)\,\omega_b k_s} & \text{PI} \\[3mm] \dfrac{k_s \left(1 + s\tau_z\right) s}{2H\left(1 + s\tau_p\right)s^2 + \omega_b k_s \left(1 + s\tau_z\right)} & \text{LL} \\[3mm] \dfrac{k_s s}{2Hs^2 + D_p HP(s)s + k_s \omega_b} & \text{HP} \end{cases}$$

$$(44)$$

Inertial Effect

$$\frac{\Delta P_v}{s\Delta \omega_g} =$$

$$\begin{cases} -\dfrac{2Hk_s\omega_b s + D_p k_s \omega_b}{2Hs^3 + D_p s^2 + k_s \omega_b s} & \text{Droop} \\[3mm] -\dfrac{\omega_b k_s \left(2Hs^2 + D_{PLL}s - PLL(s)D_{PLL}\omega_b\right)}{2Hs^4 + D_{PLL}s^3 + k_s \omega_b \left(1 - k_g PLL(s)D_{PLL}\right)s} & \text{PLL} \\[3mm] -\dfrac{2HE_0V_0\omega_b}{2HZ_q s^2 + E_0 V_0 \omega_b} & \text{RQ} \\[3mm] -\dfrac{k_s \omega_b}{s^2 + (k_d s + k_h)\,\omega_b k_s} & \text{PI} \\[3mm] -\dfrac{2H\omega_b k_s \left(1 + s\tau_p\right)}{2H\left(1 + s\tau_p\right)s^2 + \omega_b k_s \left(1 + s\tau_z\right)} & \text{LL} \\[3mm] -\dfrac{2Hk_s\omega_b s + D_p HP(s) k_s \omega_b}{2Hs^3 + D_p HP(s)s^2 + k_s \omega_b s} & \text{HP} \end{cases}$$

$$(43)$$

Step Response to Active Power Reference Variation

$$\frac{\Delta P_v}{\Delta P_v^*} =$$

$$\begin{cases} \dfrac{k_s \omega_b}{2Hs^2 + D_p s + k_s \omega_b} & \text{Droop} \\[3mm] \dfrac{k_s \omega_b}{2Hs^2 + D_{PLL}s + k_s \omega_b (1 - k_g PLL(s)D_{PLL})} & \text{PLL} \\[3mm] \dfrac{E_0 V_0 \omega_b}{2HZ_q s^2 + E_0 V_0 \omega_b} & \text{RQ} \\[3mm] \dfrac{(k_d s + k_h)\,k_s \omega_b}{s^2 + (k_d s + k_h)\,\omega_b k_s} & \text{PI} \\[3mm] \dfrac{\left(1 + s\tau_p\right) k_s \omega_b}{2H\left(1 + s\tau_p\right)s^2 + \omega_b k_s \left(1 + s\tau_z\right)} & \text{LL} \\[3mm] \dfrac{k_s \omega_b}{2Hs^2 + D_p HP(s)s + k_s \omega_b} & \text{HP} \end{cases}$$

$$(45)$$

This article has been accepted for publication in IEEE Transactions on Industry Applications. This is the author's version which has not been fully edited and content may change prior to final publication. Citation information: DOI 10.1109/TIA.2023.3293779

14

REFERENCES

[1] M. Chen, D. Zhou, and F. Blaabjerg, "Modelling, Implementation, and Assessment of Virtual Synchronous Generator in Power Systems," *Journal of Modern Power Systems and Clean Energy*, vol. 8, no. 3, pp. 399–411, May 2020.

[2] M. Shadoul, R. Ahshan, R. S. AlAbri, A. Al-Badi, M. Albadi, and M. Jamil, "A Comprehensive Review on a Virtual-Synchronous Generator: Topologies, Control Orders and Techniques, Energy Storages, and Applications," *Energies*, vol. 15, no. 22, p. 8406, Jan. 2022.

[3] M. Ebrahimi, S. A. Khajehoddin, and M. Karimi-Ghartemani, "An Improved Damping Method for Virtual Synchronous Machines," *IEEE Transactions on Sustainable Energy*, vol. 10, no. 3, pp. 1491–1500, Jul. 2019.

[4] P. Kundur, *Power System Stability and Control*. McGraw-Hill Education, Jan. 1994.

[5] Q.-C. Zhong and G. Weiss, "Synchronverters: Inverters That Mimic Synchronous Generators," *IEEE Transactions on Industrial Electronics*, vol. 58, no. 4, pp. 1259–1267, Apr. 2011.

[6] S. D'Arco, J. A. Suul, and O. B. Fosso, "A Virtual Synchronous Machine implementation for distributed control of power converters in SmartGrids," *Electric Power Systems Research*, vol. 122, pp. 180–197, May 2015.

[7] M. Chen, D. Zhou, and F. Blaabjerg, "Active Power Oscillation Damping Based on Acceleration Control in Parallel Virtual Synchronous Generators System," *IEEE Transactions on Power Electronics*, pp. 1–1, 2021.

[8] H. Beck and R. Hesse, "Virtual synchronous machine," in *2007 9th International Conference on Electrical Power Quality and Utilisation*, Oct. 2007, pp. 1–6.

[9] F. Mandrile, E. Carpaneto, and R. Bojoi, "Virtual Synchronous Generator with Simplified Single-Axis Damper Winding," in *2019 IEEE 28th International Symposium on Industrial Electronics (ISIE)*, Jun. 2019, pp. 2123–2128.

[10] L. Huang, H. Xin, H. Yuan, G. Wang, and P. Ju, "Damping Effect of Virtual Synchronous Machines Provided by a Dynamical Virtual Impedance," *IEEE Transactions on Energy Conversion*, pp. 1–1, 2020.

[11] L. Harnefors, M. Hinkkanen, U. Riaz, F. M. M. Rahman, and L. Zhang, "Robust Analytic Design of Power-Synchronization Control," *IEEE Transactions on Industrial Electronics*, vol. 66, no. 8, pp. 5810–5819, Aug. 2019.

[12] A. Narula, M. Bongiorno, M. Beza, and P. Chen, "Tuning and evaluation of grid-forming converters for grid-support," in *2021 23rd European Conference on Power Electronics and Applications (EPE'21 ECCE Europe)*. Ghent, Belgium: IEEE, Sep. 2021, pp. P.1–P.10.

[13] Y. Tao, Y. Deng, G. Li, G. Chen, and X. He, "Evaluation and Comparison of the Low-Frequency Oscillation Damping Methods for the Droop-Controlled Inverters in Distributed Generation Systems," *Journal of Power Electronics*, vol. 16, no. 2, pp. 731–747, Mar. 2016.

[14] C. Sun, G. Joos, and F. Bouffard, "Identification of low-frequency oscillation mode and improved damping design for virtual synchronous machines in microgrid," *IET Generation, Transmission & Distribution*, vol. 13, no. 14, pp. 2993–3001, Jul. 2019.

[15] W. Zhang, D. Remon, and P. Rodriguez, "Frequency support characteristics of grid-interactive power converters based on the synchronous power controller," *IET Renewable Power Generation*, vol. 11, no. 4, pp. 470–479, 2017.

[16] F. Mandrile, E. Carpaneto, and R. Bojoi, "Grid-Feeding Inverter With Simplified Virtual Synchronous Compensator Providing Grid Services and Grid Support," *IEEE Transactions on Industry Applications*, vol. 57, no. 1, pp. 559–569, Jan. 2021.

[17] F. Mandrile, V. Mallemaci, E. Carpaneto, and R. Bojoi, "A Lead-Lag Filter for Virtual Synchronous Machines with Improved Electromechanical Damping," in *2021 IEEE Energy Conversion Congress and Exposition (ECCE)*, Oct. 2021, pp. 583–589.

[18] F. Mandrile, E. Carpaneto, E. Armando, and R. Bojoi, "Simple Tuning Method of Virtual Synchronous Generators Reactive Control," in *2020 IEEE Energy Conversion Congress and Exposition (ECCE)*, Oct. 2020, pp. 2779–2785.

[19] F. Mandrile, E. Carpaneto, and R. Bojoi, "VSG Simplified Damper Winding: Design Guidelines," in *IECON 2019 - 45th Annual Conference of the IEEE Industrial Electronics Society*, vol. 1, Oct. 2019, pp. 3962–3967.

[20] X. Yan and S. Y. A. Mohamed, "Comparison of virtual synchronous generators dynamic responses," in *2018 IEEE 12th International Conference on Compatibility, Power Electronics and Power Engineering (CPE-POWERENG 2018)*, Apr. 2018, pp. 1–6.

[21] H. Bevrani, T. Ise, and Y. Miura, "Virtual synchronous generators: A survey and new perspectives," *International Journal of Electrical Power & Energy Systems*, vol. 54, pp. 244–254, Jan. 2014.

[22] H. Yin, Z. Kustanovich, and G. Weiss, "Attenuation of power system oscillations by using virtual damper windings," in *2022 IEEE 23rd Workshop on Control and Modeling for Power Electronics (COMPEL)*, Jun. 2022, pp. 1–6.

[23] Z. Kustanovich, S. Shivratri, H. Yin, F. Reissner, and G. Weiss, "Synchronverters With Fast Current Loops," *IEEE Transactions on Industrial Electronics*, pp. 1–10, 2022, (Early Access).

[24] V. Mallemaci, F. Mandrile, S. Rubino, A. Mazza, E. Carpaneto, and R. Bojoi, "A comprehensive comparison of Virtual Synchronous Generators with focus on virtual inertia and frequency regulation," *Electric Power Systems Research*, vol. 201, p. 107516, Dec. 2021.

[25] N. Tleis, *Power Systems Modelling and Fault Analysis*. Elsevier, 2019.

[26] J. Liu, Y. Miura, and T. Ise, "Comparison of Dynamic Characteristics Between Virtual Synchronous Generator and Droop Control in Inverter-Based Distributed Generators," *IEEE Transactions on Power Electronics*, vol. 31, no. 5, pp. 3600–3611, May 2016.

[27] M. Li, Y. Wang, N. Xu, Y. Liu, W. Wang, H. Wang, and W. Lei, "A novel virtual synchronous generator control strategy based on improved swing equation emulating and power decoupling method," in *2016 IEEE Energy Conversion Congress and Exposition (ECCE)*, Sep. 2016, pp. 1–7.

Fabio Mandrile (S'18, M'21) received the M.Sc. and Ph.D. degrees in electrical engineering from Politecnico di Torino, Italy, in 2017 and 2021, respectively. He is currently assistant professor at Dipartimento Energia "G. Ferraris" at Politecnico di Torino. His main research interests are virtual synchronous machines and power electronics for grid-connected applications, on which he focused his Ph.D. and current research activity.

Vincenzo Mallemaci (S'20) was born in Messina, Italy, in 1996. He received the Bachelor and Master degrees both in electrical engineering from Politecnico di Torino, Italy, in 2018 and 2020, respectively. He is currently a Ph.D. student at Dipartimento Energia "G. Ferraris" at Politecnico di Torino. His Ph.D. activity focuses on virtual synchronous machines and control for power electronic grid–connected converters.

Enrico Carpaneto (M'86) was born in Torino, Italy, in 1959. He received the M.Sc. and Ph.D. degrees in electrical engineering from Politecnico di Torino, Torino, Italy, in 1984 and 1989, respectively. He is currently an Associate with the Energy Department, Politecnico di Torino. His research activities cover many different aspects of modeling, simulation and optimization of generation, transmission and distribution systems. He has published more than 100 scientific papers. He has been responsible for several research contracts concerning analysis, operation and planning of distribution networks, power quality, and generation optimization. His current research interests include distribution systems, dispersed generation, virtual synchronous generators, and thermal models. Dr. Carpaneto is a member of the IEEE Power Engineering Society and Associazione Italiana di Elettrotecnica, Elettronica, Automazione, Informatica e Telecomunicazioni (AEIT).

Radu Bojoi (SM'10, F'19) received the M.Sc. degree from Technical University of Iasi, Romania, in 1993, and the Ph.D. degree from Politecnico di Torino, Torino, Italy, in 2002, all in electrical engineering. He is a Full Professor of Power Electronics and Electrical Drives with the Energy Department G. Ferraris and Chairman of the Power Electronics Innovation Center, Politecnico di Torino. He has authored or coauthored more than 150 papers covering electrical drives and power electronics for industrial applications, transportation electrification, power quality, and home appliances. He was involved in many research projects with industry for direct technology transfer aiming at obtaining new products. Prof. Bojoi is the co-recipient of five prize paper awards, the last one in 2015 as IEEE-IAS Prize Paper Award. Dr. Bojoi is a Co-Editor-In-Chief of the IEEE Transactions on Industrial Electronics.